



Cite this: DOI: 10.1039/d5pm00189g

## The effect of guide RNA thermal denaturation on the quality of Cas9 ribonucleoprotein-loaded lipid nanoparticle formulations

Rina Shimizu,<sup>a</sup> Yuji Kashiwakura,<sup>b,c</sup> Morisada Hayakawa,<sup>b,c</sup> Shunsuke Kita,<sup>d</sup> Mina Sato,<sup>e</sup> Masatoshi Maeki,<sup>f</sup> Manabu Tokeshi,<sup>f</sup> Katsumi Maenaka,<sup>f</sup> Tsukasa Ohmori,<sup>b,c</sup> Yuma Yamada,<sup>d</sup> <sup>a,e</sup> Hideyoshi Harashima<sup>e</sup> and Yusuke Sato <sup>d</sup> <sup>\*a,e</sup>

Gene-editing technology for the treatment of genetic diseases uses a system that delivers clustered regularly interspaced short palindromic repeats (CRISPR)/CRISPR-associated (Cas) 9 as ribonucleoproteins (RNPs) in a faster and more transiently effective manner than other delivery methods that involve gene expression. Lipid nanoparticles (LNPs) are an integral part of technology that is used to deliver Cas9 RNPs, and in recent years the *in vivo* delivery of RNPs has been achieved. While single-guide RNA (sgRNA) forms complex higher-order structures, which are known to result in the formation of heterogeneous RNPs, the impact on RNP-loaded LNP formulations has been overlooked. The results of this study show that the heterogeneity of sgRNA significantly affects the internal structure, physical properties, and knockout activity of RNP-loaded LNP formulations through changes in molecular weight distribution and RNP charge.

Received 18th July 2025,  
Accepted 14th October 2025

DOI: 10.1039/d5pm00189g

rsc.li/RSCPharma

## 1. Introduction

Genome editing has enabled fundamental treatment of genetic diseases *via* the ability to modify genomic DNA sequences of interest. In particular, the development of clustered regularly interspaced short palindromic repeats (CRISPR)/CRISPR-associated (Cas) 9 technology was first reported in 2012. This development accelerated the advancement of genome editing research and is responsible for the broad applications that followed.<sup>1–4</sup> CRISPR/Cas9 works as a complex of Cas9 proteins and single-guide RNAs (sgRNAs) that guide Cas9 proteins to a target sequence. RNA-based targeting

has enabled simplified, low-cost, and highly effective genome editing,<sup>5</sup> but one of the challenges facing this technology is the need to efficiently and specifically deliver CRISPR/Cas9 to target cells and tissues for therapeutic applications.<sup>6</sup>

To overcome this challenge, various delivery systems have been developed. The adeno-associated virus (AAV) vector is one of the most used *in vivo* delivery techniques for genome editing.<sup>7–10</sup> However, side effects such as the integration of viral DNA into the genome, or immunogenicity, limits the load capacity and presence of neutralizing antibodies and is a significant problem that must be overcome.<sup>11–13</sup> Lipid nanoparticles (LNPs) are a class of non-viral vectors that have the potential to conquer viral DNA. LNPs are used to cover nucleic acids and proteins to enable their passage through cell membranes.<sup>6,14,15</sup> NTLA-2001 (nexiguran ziclemeran) is a candidate for RNA-loaded LNP-based *in vivo* genome editing therapy that is being examined for use in the treatment of transthyretin (TTR) amyloidosis.<sup>16</sup> This regimen currently is in phase III clinical trials. The same technology, NTLA-2002, has been applied to the treatment of hereditary angioedema (HAE) by targeting the KLKB1 gene that encodes the kallikrein B1 protein. Alternatively, the delivery of ribonucleoproteins (RNPs), a complex of Cas9 proteins and sgRNAs, is now being investigated. This strategy skips the transcription, translation, and complexation processes. Therefore, this regimen is thought to be an efficient approach.<sup>17,18</sup> Although research on

<sup>a</sup>Laboratory for Molecular Design of Pharmaceutics, Faculty of Pharmaceutical Sciences, Hokkaido University, Hokkaido, 060-0812, Japan.

E-mail: y\_sato@pharm.hokudai.ac.jp

<sup>b</sup>Department of Biochemistry, Jichi Medical University School of Medicine, 3311-1 Yakushiji, Shimotsuke, Tochigi 329-0498, Japan

<sup>c</sup>Center for Gene Therapy Research, Jichi Medical University, 3311-1 Yakushiji, Shimotsuke, Tochigi 329-0498, Japan

<sup>d</sup>Laboratory of Biomolecular Science and Center for Research and Education on Drug Discovery, Faculty of Pharmaceutical Sciences, Hokkaido University, Kita-12 Nishi-6, Kita-ku, Sapporo 060-0812, Japan

<sup>e</sup>Laboratory of Innovative Nanomedicine, Faculty of Pharmaceutical Sciences, Hokkaido University, Kita-12 Nishi-6, Kita-ku, Sapporo 060-0812, Japan

<sup>f</sup>Division of Applied Chemistry, Faculty of Engineering, Hokkaido University, Kita-13 Nishi-8, Kita-ku, Sapporo 060-8628, Japan



RNP delivery is ongoing, the number of in-depth examinations and optimization studies remains limited.

Indeed, there is no established protocol for the formation of RNPs. In particular, factors such as sequence and secondary and tertiary structures of sgRNAs are known to affect the formation of complexes with Cas9 and enzymatic activities.<sup>19–21</sup> However, the relationship between sgRNA structures and RNP formations remains incompletely understood. Previous reports on the structural analysis of sgRNAs have used size exclusion chromatography (SEC),<sup>22</sup> FLET assays,<sup>23</sup> circular dichroism,<sup>24</sup> crystal structure analyses,<sup>25–27</sup> and cryo-electron microscopy.<sup>28</sup> In addition, there has been structural analysis into how RNPs are related to sgRNAs.<sup>27–29</sup> However, these methods have been limited to the qualitative analysis of sgRNAs, and an optimized structure that could account for both formulation and delivery processes as well as the relationship between structure and *in vivo* activity remains unclear.

In this study, we report the impact that the heterogeneity of sgRNAs exerts on the internal structure, physical properties, and knockout activity of RNP-loaded LNP formulations through changes in both the molecular weight distribution and charge density of RNPs. In addition, RNP-loaded LNPs with denatured sgRNAs exhibit resistance to cryopreservation and have induced obvious gene knockouts in neonatal mice, which has introduced the possibility of applications to the treatment of genetic diseases.

## 2. Results and discussion

### 2.1 Thermal denaturation of sgRNAs

Sequence-dependent differences in the RNA higher-order structure of sgRNAs have been reported to have a significant impact on their complexation with Cas9, *i.e.*, the efficiency of RNP formation and target DNA cleavage activity.<sup>28</sup> RNA folds upon synthesis and takes on a secondary structure that is capable of binding Cas9, but this structure differs from that of the active form.<sup>29</sup> This alters the DNA cleavage activity. The secondary structure of sgRNAs could be a factor that should not be ignored in aiming for higher levels of genome editing efficiency, since activity is restored for at least some sgRNAs following the disruption of internal interactions *via* thermal denaturation. In addition, chemically synthesized multimeric sgRNAs are known to form inactive aggregates by binding to Cas9.<sup>22</sup> On the other hand, the effects of both secondary structures and multimerization of sgRNAs on nanoparticle formulations delivering Cas9 RNPs remain unclear. Therefore, in this study, homogenization of the higher-order structure of sgRNAs *via* thermal denaturation was examined for its effect on the structure and activity of Cas9 RNP-loaded LNPs.

First, the changes in the molecular weight distribution and in the secondary structure of sgRNAs with or without thermal denaturation were examined *via* native-PAGE and circular dichroism (CD) spectroscopy, respectively, in order to track the structural changes of sgRNAs caused by thermal denaturation. The band pattern of end-modified sgTTR-G211,<sup>30</sup> an sgRNA

against mouse transthyretin (TTR), was markedly different with or without thermal denaturation, and thermal denaturation tends to result in the concentration of a single band that could be considered a monomer (Fig. 1A). Results similar to native-PAGE were obtained *via* capillary electrophoresis of sgTTR-G211 (SI Fig. S1). The monomeric band of the thermally denatured sgTTR-G211 was clearly retained even after three freeze-thaw cycles (SI Fig. S2), which suggests that thermally denatured sgRNA could be stored frozen. In addition, consistent results were observed on *in vitro*-transcribed sgTTR-G211 (SI Fig. S3). The fact that the weak band was found in a position close to the monomer in sgRNA without thermal denaturation suggests that the proportion of the secondary structure that remains identical to that following heat denaturation is limited. Similar changes were also observed in end-modified sgRNAs for murine coagulation factor VIII (FVIII) or murine proprotein convertase subtilisin/kexin type 9 (PCSK9) (SI Fig. S4). Collectively, the results of this study showed that chemically synthesized end-modified sgRNAs exhibit heterogeneous higher-order structures, despite the different genomic target sequences. By contrast, the highly modified sgTTR-G211 was obviously a homogeneous monomer even without thermal denaturation (SI Fig. S4). This suggests that chemical modifications inside the sgRNA could facilitate the formation of highly active secondary structures. On the other hand, it is difficult to conclude the existence of such a development, as it remains possible that post-chemical synthesis processing is not identical between the highly modified and end-modified forms of sgTTR-G211. Nevertheless, considering that chemically synthesized end-modified or unmodified sgRNAs rather than highly modified sgRNAs or *in vitro*-transcribed gRNAs are commonly used in genome editing *via* RNP delivery.<sup>31,32</sup> In addition, the fact that all the end-modified sgRNAs examined in this study have a heterogeneous higher-order structure without thermal denaturation is an issue that cannot be ignored in the production of RNP-loaded LNP formulations. In subsequent experiments, end-modified sgTTR-G211 was used.

The sgRNAs showed negative and positive bands at approximately 210 and 265 nm, respectively, qualitatively indicating an A-type helix.<sup>33–36</sup> No obvious changes in the CD spectra were observed with or without thermal denaturation (Fig. 1B). On the other hand, the negative band at 207 nm was significantly reduced by thermal denaturation, while the positive band at 267 nm was only slightly reduced by thermal denaturation (Fig. 1C and D). The bands at about 210 and 265 nm are attributed to base-pair interactions and also to the hairpin structure. The reduction of bands by thermal denaturation in both wavelength ranges suggests relative denaturation, which is a result that is consistent with the resolution of multimerization by thermal denaturation.

### 2.2 Effect that the thermal denaturation of sgRNAs exerts on the physical properties of RNP-loaded LNPs

We previously found that CL4F11- $\zeta$ -2 (denoted as  $\zeta$ ) is an ionizable lipid that enables efficient *in vivo* delivery of Cas9 RNPs.<sup>37</sup> The RNP-loaded  $\zeta$ -LNPs exhibited a characteristic



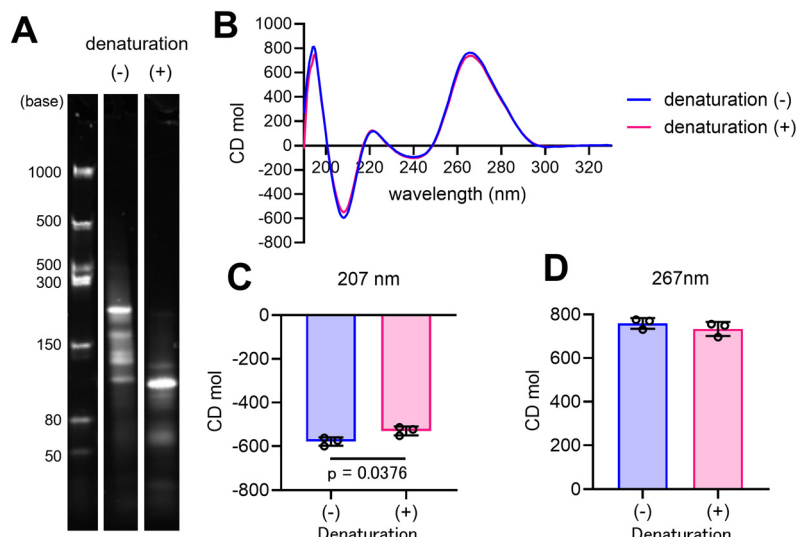


**Fig. 1** Effect of thermal denaturation on molecular weight and secondary structure of sgRNAs. (A) Native PAGE of end-modified sgTTR-G211. (B) CD spectra of end-modified sgTTR-G211. (C and D) Band peak of the CD spectra at 207 nm (C) and 267 nm (D).  $n = 3$  technically independent measurements per each condition.

flower-like structure with multiple blebs around an electron-dense core, which implies a heterogeneous distribution of LNP components. On the other hand, short interfering RNA (siRNA)-loaded  $\zeta$ -LNPs show no such flower-like structure, suggesting that the RNPs were responsible for the heterogeneity of the formulation.<sup>37</sup> As reported previously, single-stranded oligo deoxy nucleotides (ssODNs) with partial complementary sequences to the genomic target sequence of the sgRNA were added to the RNPs to improve RNP encapsulation into the LNPs, which is driven by electrostatic interactions with positively charged ionizable lipids.<sup>38,39</sup> Thermal denaturation resulted in a slight decrease (10%) in the particle sizes of the RNP-loaded LNPs and in a marked improvement in RNP encapsulation efficiency (Fig. 2A and SI Table S1). Furthermore, cryoTEM observations revealed that thermal denaturation of sgRNA significantly reduced the number of blebs in the RNP-loaded LNPs and improved their homogeneity (Fig. 2B, C and SI Fig. S5, S6). Considering the payload-

dependent differences in particle structure observed in previous studies,<sup>37,40</sup> the apparent changes in particle structure with or without thermal denaturation of sgRNA strongly suggests differences in the RNP structure.

### 2.3 RNP structural diversity analysis

As mentioned above, non-thermally denatured sgRNAs are known to induce the formation of multimeric RNPs,<sup>22</sup> because it is assumed that multimeric RNPs could differ from the expectations for monomeric RNPs in terms of complex properties that affect the efficiency of encapsulation onto LNPs. Therefore, we focused on characterizing RNPs.

First, the effect that the thermal denaturation of sgRNA exerts on the molecular weight distribution of RNPs was verified *via* mass photometry, which enables quantitative analysis of the molecular weight of macromolecules at the single-molecule level in solution in a label-free manner. Surprisingly, only approximately 27% of the RNP molecules in the non-thermally

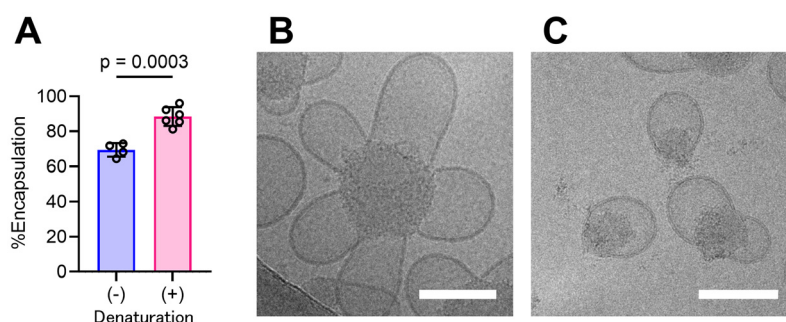


**Fig. 2** Effect of thermal denaturation of sgRNA on physicochemical characterization of RNP-loaded LNPs. (A) Effect of thermal denaturation on RNP encapsulation efficiency.  $n = 4\text{--}6$  technically independent measurements per each condition. (B and C) Cryo-TEM observation of RNP-loaded LNPs. The sgRNAs without (B) or with (C) thermal denaturation were used. Bars represent 100 nm.



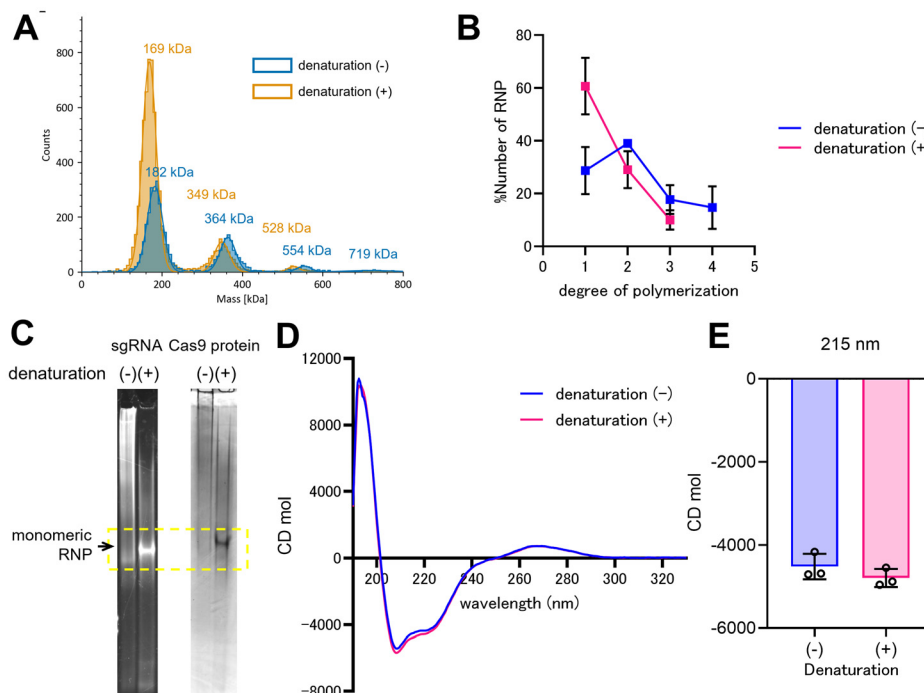


**Fig. 3** Effect of thermal denaturation of sgRNAs on physicochemical characterization of RNPs. (A) Molecular weight distribution of RNPs measured by mass photometry. (B) Percentage of RNP molecules at each degree of polymerization determined by mass photometry.  $n = 3$  technically independent measurements per each condition. (C) Native PAGE of RNPs. The sgRNA (left) or Cas9 protein (right) was stained and visualized. (D) CD spectra of RNPs. (E) Band peak of the CD spectra at 215 nm.  $n = 3$  technically independent measurements per each condition.

denatured sample were of the monomeric RNP type, while more than 70% formed dimers or larger multimers (Fig. 3A and B). On the other hand, in thermally denatured sgRNA-RNPs, the share of monomeric RNPs increased to approximately 60% and approximately 90% of total RNP molecules had formed dimers and less, which suggests that the thermal denaturation of sgRNAs causes a significant change in the structure of RNPs and improves their homogeneity. A consistent result was obtained for end-modified sgPCSK9-Cas9 RNPs, which indicates generality (SI Fig. S7). Consistent results were also obtained for ssODN-sgTTR-G211-RNPs (SI Fig. S8). RNP aggregation is known to occur particularly when the stoichiometry ratio of the sgRNAs for Cas9 is less than 1. Varying the stoichiometric ratio from 0.8 to 1.5 gradually increased the monomeric RNP fraction (up to 84%), while the multimeric RNP did not disappear (SI Fig. S9), which suggests that the presence of multimeric RNP in thermally denatured sgRNAs was not inherently attributable to fluctuations in the stoichiometric ratio due to experimental error. Wei *et al.* increased the stoichiometry of sgRNAs for Cas9 protein three-fold to enhance the negative charge of RNPs and facilitate their loading onto LNPs.<sup>17</sup> Indeed, an increase in the stoichiometry of thermally denatured sgRNA improved the yield of monomeric RNPs, and an approximately 30 kDa increase in the average molecular weight of monomeric RNPs (SI Fig. S9) suggests the binding of two molecules of sgRNA to one Cas9 protein. The process of Blue native (BN)-PAGE showing the

thermal denaturation of sgRNA also revealed an increase in the stoichiometry of sgRNA that decreased the average molecular weight of RNPs (SI Fig. S10). These results clearly indicate that thermal denaturation of sgRNA contributes to both a reduction and the homogenization of the RNP molecular weight distribution, which complicates a direct explanation for the improvement in RNP encapsulation efficiency and for changes in the particle structure. Indeed, LNPs are known to efficiently encapsulate larger complexes of both mRNA (*e.g.*, approximately 1300 kDa at 4000 nt) and pDNA (*e.g.*, approximately 3800 kDa at 6000 bp) compared with that of multimeric RNPs (several hundred kDa). It is well known that the encapsulation of payloads such as nucleic acids is driven mainly by electrostatic interactions with ionizable lipids,<sup>41,42</sup> and, therefore, it was assumed that the thermal denaturation of sgRNA would affect the charge of RNPs. Indeed, non-thermally denatured sgRNA-RNPs showed a broad distribution in native-PAGE in the region of a short migration distance, whereas thermally denatured sgRNA-RNPs showed a relatively sharp distribution near the center. That result suggests that the thermal denaturation of sgRNAs enhances the negative charge of the RNPs (Fig. 3C). The increased stoichiometry of the heat-denatured sgRNA resulted in a clear increase in charge density (SI Fig. S11), which is consistent with the binding of two molecules of sgRNA, as suggested by mass photometry.

The RNPs produced CD spectra that qualitatively indicates an  $\alpha$ -helix-rich structure (Fig. 3D), which is consistent with pre-



vious reports from the X-ray crystallography of Cas9 RNPs complexed with target DNA<sup>25</sup> regardless of the heat denaturation of sgRNA. The negative band at 210 nm for RNP tended to increase *via* the thermal denaturation of sgRNA (Fig. 3E). Although spyCas9 is known to be inactive as a nuclease on its own due to a tightly interacting structure of two lobes referred to as the  $\alpha$ -helical and RuvC lobes,<sup>43,44</sup> the two lobes rotate significantly ( $\sim 100^\circ$ ) as the folding of the bridge helix is resolved *via* binding to gRNA.<sup>45</sup> Although the detailed structure is unknown, it is possible that the above-mentioned conformational changes in the Cas9 protein were affected by the thermal denaturation of sgRNA. As the Cas9 protein itself does not have dimers (SI Fig. S12), the differences in the molecular weight distribution and in the charge density of the RNPs derive from the heterogeneity of the sgRNA.

#### 2.4 Evaluation of DNA cleavage activity

The target DNA cleavage activity of RNPs could differ depending on the thermal denaturation of sgRNAs. Camperi *et al.* reported that multimeric RNPs generated by non-thermally denatured sgRNAs are enzymatically inactive.<sup>22</sup> First, the DNA cleavage activity of RNPs at 37 °C, which mimics body temperature, was examined. The cleavage efficiency increased in a stoichiometric dependence on the target DNA, and no change in activity due to thermal denaturation of sgRNA was observed (Fig. 4A). Since the multimeric RNPs could be activated by the resolution of sgRNA during incubation at 37 °C, the DNA cleavage activity at a relatively low temperature of 15 °C was subsequently examined. As with the result at 37 °C, no difference in activity due to thermal denaturation of sgRNA was observed (Fig. 4B). The disappearance of the upper bands, which were assumed to be derived from the multimers, was observed only at 70 °C (SI Fig. S13). Consistent results were observed for different sgRNAs (SI Fig. S4). Considering previous reports showing increased activity of RNPs *via* the thermal denaturation of sgRNAs,<sup>29</sup> it cannot be assumed that sgRNAs were denatured during the reaction at 15 °C. Contrary to previous

reports, it is clear that the multimeric RNPs in this study retained their target DNA cleavage activity.

#### 2.5 Evaluation of pharmacokinetics and *in vivo* KO activity of RNP-loaded LNPs

Thermal denaturation of sgRNA did not affect the target DNA cleavage activity of RNPs, but it did alter the particle size, the particle structure, and the RNP encapsulation ratio of the RNP-loaded LNPs. Therefore, thermal denaturation of sgRNA could alter the potency of RNP-loaded LNPs *in vivo*. Initially, the distribution of RNP-loaded LNPs in the liver after intravenous administration was observed. Non-thermally denatured sgRNA-RNP-loaded LNPs localized mainly to liver sinusoidal endothelial cells (LSECs), whereas thermally denatured sgRNA-RNP-loaded LNPs showed improved accumulation in the hepatocytes surrounded by blood vessels, which are the target cells for TTR knockout (Fig. 5A). The TTR knockout activity was subsequently assessed using the serum TTR protein concentration as an indicator. A single dose of the RNP-loaded LNPs at 0.2 mg RNP kg<sup>-1</sup> resulted in a significant decrease in serum TTR concentration, which was significantly enhanced by thermal denaturation of the sgRNA (Fig. 5B). In conclusion, thermal denaturation of sgRNAs enhanced both the accumulation to hepatocytes and the gene knockout activity of RNP-loaded LNPs. As mentioned above, thermal denaturation of sgRNA reduced the particle size of the RNP-loaded particles. Access to hepatocytes requires penetration of the numerous small pores (fenestra) in the LSECs, and a reduction in particle size contributes to an increase in their penetration efficiency.<sup>46,47</sup> However, the rate of reduction in particle size was slight and its impact was considered limited. Thermal denaturation of sgRNAs also significantly altered the particle structure of the RNP-loaded LNPs. In our previous study, non-thermally denatured sgRNA-RNP-loaded LNPs exhibited a flower-like structure and induced gene knockout in an ApoE-independent manner, unlike the corresponding siRNA-loaded LNPs.<sup>37</sup> The large number of blebs is assumed

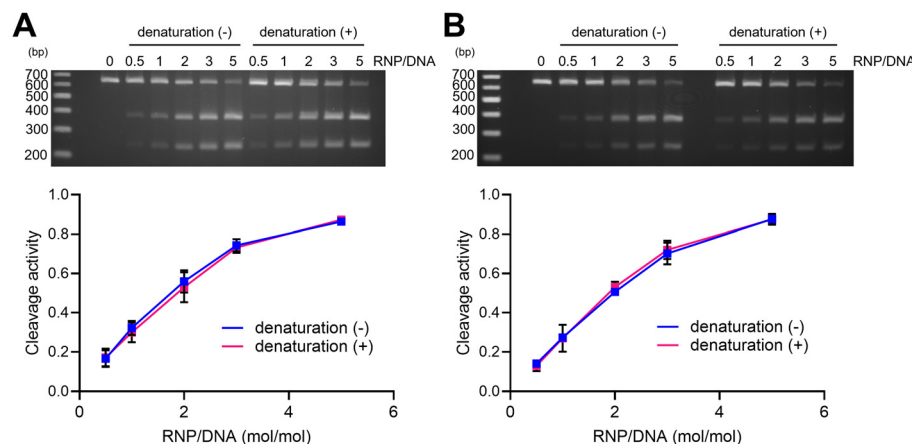


**Fig. 4** Effect of thermal denaturation of sgRNAs on enzymatic activity of RNPs. DNA cleavage activity of RNPs at 37 °C (A) or 15 °C (B) was measured.  $n = 3$  technically independent measurements per each condition.



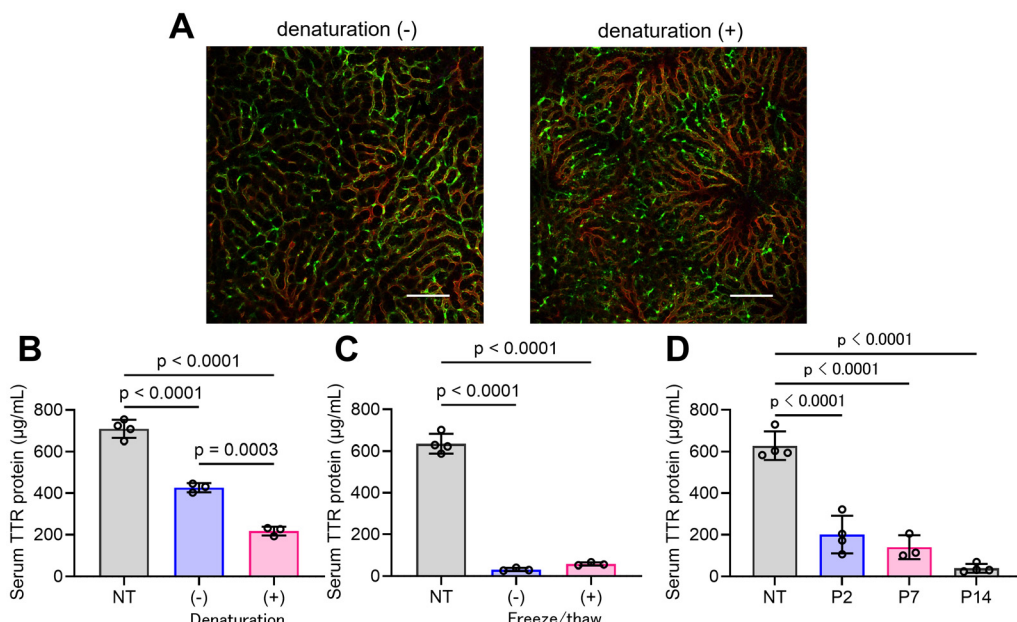


**Fig. 5** *In vivo* performance of thermally denatured sgRNA-RNP-loaded LNPs. (A) Effect of thermal denaturation of sgRNA on intrahepatic distribution of RNP-loaded LNPs. Green and red represent LNPs and blood vessels, respectively. Bars represent 200  $\mu$ m. (B) Effect of thermal denaturation of sgRNA on knockout activity of freshly prepared RNP-loaded LNPs. Mice were injected with the LNPs at a dose of 0.2 mg RNP kg $^{-1}$ . (C) Freeze–thaw tolerance of the thermally denatured sgRNA-RNP-loaded LNPs. Mice were injected with the LNPs at a dose of 1 mg RNA kg $^{-1}$ . (D) Knockout activity of the thermally denatured sgRNA-RNP-loaded LNPs in neonatal mice. The mice were injected with the LNPs at a dose of 1 mg RNA kg $^{-1}$ .  $n = 3$ –4 technically independent measurements per each condition.

to be due to incomplete RNP encapsulation (*i.e.*, partial exposure of RNPs to the particle surface). As RNPs themselves selectively accumulate in LSECs,<sup>39</sup> improved RNP encapsulation could have reduced the migration to LSECs through a reduction in the LSEC-tropic RNPs exposed to the particle surface. It is also possible that the thermal denaturation of sgRNAs could have enhanced hepatocyte accumulation by altering the corona proteins.<sup>48</sup> Since exposure of RNPs to the LNP surface could lead to its degradation in the blood,<sup>49</sup> improving RNP encapsulation efficiency could simply protect RNPs from degradation and contribute to enhanced gene knockout activity. In addition, an increase in the proportion of monomeric RNPs could increase their potency *in vivo*, because it is conceivable that multimeric RNPs cleaved the target DNA *in vitro*. Monomeric RNPs, however, are potentially less efficient in translocation from the cytoplasm to the nucleus *in vivo*.<sup>50,51</sup> In any case, thermal denaturation of sgRNA is an important process to consider and control in the development of RNP delivery formulations, as it improves formulation uniformity and gene-knockout activity.

Storage stability is important for clinical applications of RNP-loaded LNPs. No significant changes in physical properties were observed in RNP-loaded  $\zeta$ -LNPs for up to two weeks (SI Table S2). On the other hand, the spyCas9 protein is known to be thermodynamically unstable and is denatured at 45 °C.<sup>49,52</sup> In fact, in our previous study, spyCas9 RNP-loaded LNPs maintained knockout activity for up to two weeks at 4 °C, but a clear decline was observed after four weeks.<sup>38</sup> Although

Cas proteins with improved thermostability, such as *Geobacillus stearothermophilus* Cas9 (GeoCas9), have been developed,<sup>18,49</sup> spyCas9 is overwhelmingly used in basic research and is increasingly being applied to humans, which means it could still be important.<sup>16,53</sup> Therefore, the freeze–thaw tolerance of the RNP-loaded LNPs was examined assuming cryopreservation as with the COVID-19 mRNA vaccines.<sup>54–56</sup> The RNP-loaded LNPs showed no significant change in physical properties even after three freeze–thaw cycles, which suggests that it has sufficient tolerability to a single freeze–thaw cycle (SI Table S3). Single-particle analyses *via* NanoFCM showed no change in either particle-size distribution or the proportion of RNP-loading particles due to freeze–thawing (SI Fig. S14). Furthermore, no significant reduction in gene knockout activity *in vivo* was observed (Fig. 5C). These results indicate the feasibility of using cryopreservation for RNP-loaded LNPs.

Despite the current progress in pediatric drug formulation development, clinical trials and approved drugs for the pediatric population remain limited.<sup>57</sup> Indeed, it is clear that opportunities for pediatric treatment are limited due to the small number of pediatric applications in formulations approved in the US, EU and Japan, and due to the long period of time between approval for use in adults and approval for pediatric use.<sup>58,59</sup> On the other hand, the gene therapy Lenmelyd™ that is used to treat metachromatic leukodystrophy (MLD) caused by mutations in the gene encoding the aryl-sulphatase A (ARSA) enzyme was approved by the FDA in



2024.<sup>60</sup> A workflow has recently been developed to rapidly develop customized gene editing therapies for patients with ultra-rare or unique “N-of-1” mutations.<sup>61,62</sup> This workflow has enabled the implementation of personalized gene therapy using Cas9-based, adenine-base-editor, mRNA-loaded LNP formulations for the treatment of carbamoyl phosphate synthase 1 (CPS1) deficiency, which is a severe urea cycle disorder. The N-of-1 therapy including other therapeutic modalities such as antisense nucleotides is gaining momentum and is being applied to advanced therapies in children.<sup>63</sup> Thus, the application of gene therapy and genome editing therapies to children with genetic disorders is advancing rapidly. The TTR gene knockout activity of the RNP-loaded LNPs was verified in neonatal mice, and an approximately 70–95% reduction of serum TTR protein was observed in P2–14 mice (Fig. 5D). Although genome-editing therapies for neonatal mice utilizing adeno-associated viral (AAV) vectors represent pioneering work,<sup>64</sup> the use of RNP-loaded LNPs has not yet been established—this is the first case of RNP-loaded LNPs inducing gene knockout in neonatal mice. Although challenges such as verifying pharmacokinetics and optimizing formulations remain, the results tend to validate the efficacy of applying RNP-loaded LNPs for pediatric use.

### 3. Experimental

#### 3.1 Materials

The pH-responsive cationic lipid CL4F11- $\zeta$ -2 was synthesized as described previously.<sup>37</sup> Chol was purchased from SIGMA Aldrich (St Louis, MO). The 1,2-distearoyl-sn-glycero-3-phosphocholine (DSPC) and 1,2-dimyristoyl-rac-glycero methoxyethyleneglycol 2000 ether (PEG-DMG) were obtained from the NOF Corporation (Tokyo, Japan). Recombinant spyCas9 nuclease (TrueCut Cas9 Protein v2) was purchased from Thermo Fisher Scientific (MA, USA). The end-modified sgRNAs and ssODNs were purchased from Integrated DNA Technologies, Inc. (Coralville, IA, USA), and the highly modified sgRNAs were purchased from Aji Bio-Pharma (Osaka, Japan). *In vitro* transcribed sgRNA was synthesized *via* the use of a Guide-it sgRNA *In Vitro* Transcription Kit (Takara Bio USA, Inc., San Jose, CA, USA) according to manufacturer's protocol. Sequences of sgRNAs and ssODNs are listed in the SI. An iLiNP microfluidic device was fabricated as described in a previous report.<sup>65</sup>

#### 3.2 Preparations of Cas9 RNP complex

A solution of spyCas9 protein (10  $\mu$ M) was titrated to an equal volume of each sgRNA solution (10  $\mu$ M) under vigorous mixing and incubated for 5 minutes to produce 5  $\mu$ M of an RNP solution. Depending on the experiment, different ratios of Cas9/sgRNA were mixed, in which the gRNA was either pre-denatured at 70 °C for 10 minutes and cooled down to 15 °C at a ramp rate of 1.5 °C s<sup>-1</sup> using a MiniAmp thermal cycler (Thermo Fisher Scientific) or kept at ambient temperature before each RNP formation. The RNP solution was mixed with an equal volume of an ssODN solution (5  $\mu$ M) and incubated

for 5 minutes to obtain 2.5  $\mu$ M of RNP-ssODN complexes. For the fluorescent labeling of RNPs, three molar equivalents of sulfo-Cy5-NHS was added to the RNPs and incubated for 1 h at ambient temperature in the dark.

#### 3.3 Preparations of RNP-loaded LNPs

RNP-loaded LNPs were prepared as reported previously.<sup>37</sup> An ethanol solution containing CL4F11- $\zeta$ -2, DSPC, chol, and PEG-DMG at a molar ratio of 50/10/40/3.5 was prepared with a total lipid concentration of 8 mM. For the fluorescent labeling of the LNPs, either 0.2 mol% of DiD (for *in vivo* biodistribution study) or 0.1 mol% of DiO (for nanoFCM measurement) was added to the above solution. The RNP-ssODN was diluted with 20 mM of ice-cold MES buffer (pH 6.0, 50 mM of NaCl) to reach a total volume of 160 nM. RNP-loaded LNPs were prepared by mixing the lipids in ethanol and RNP-ssODN in an aqueous solution using a polydimethylsiloxane-based iLiNP device (1 mm width) at a total flow rate of 2.0 mL min<sup>-1</sup> (0.20 mL min<sup>-1</sup> and 1.80 mL min<sup>-1</sup> for the lipid solution and the RNP-ssODN solution, respectively). A Pump 33 DDS (Dual Drive System) Syringe Pump (70-3333; Harvard Apparatus, MA, USA) was used to control the flow rate. The resultant LNP solution was dialyzed for 2 h or more at 4 °C against PBS(–) using Spectra/Por 4 dialysis membranes (molecular weight cut-off 12–14 kDa, Spectrum Laboratories, CA, USA) and was then concentrated by ultrafiltration using Amicon Ultra-15 (MWCO 100 kDa, Millipore). To evaluate tolerability against a freeze/thaw cycle, the LNP solution was dialyzed against 20 mM of Tris-HCl buffer (pH7.4) containing 9 w/v% sucrose as a cryoprotectant.

#### 3.4 Characterization of the LNPs

The size ( $\zeta$ -average), polydispersity index (PDI), and  $\zeta$ -potential of the LNPs were measured by means of a Zetasizer Nano ZS ZEN3600 instrument (Malvern Instruments, Worcestershire, UK). The LNPs were diluted in D-PBS (–) and 10 mM HEPES buffer at pH 7.4 for the measurement of size and  $\zeta$ -potential, respectively. The encapsulation efficiency (%encapsulation) and total concentration of RNP-ssODN were measured *via* Ribogreen assay, as described previously.<sup>66</sup>

RNP-loaded LNPs were added to Quantifoil Cu1.2/1.3 grids, and frozen in liquid ethane using an FEI Vitrobot MarkIV. The grids were stored in liquid nitrogen until use for imaging. A JEM-2200FS (JEOL, Japan) was used to obtain the images. The instrument was operated at 200 kV. A DE-20 camera was used to capture the images. Samples were imaged at a magnification of 30 000 $\times$ . Sample preparation and imaging was performed by Terabase Inc. (Aichi, Japan).

#### 3.5 Molecular weight analysis using mass photometry

Mass Photometry measurements were performed on thoroughly washed microscope sample carrier slides and recorded on a mass photometer (TwoMP, Refeyn Ltd, Oxford, UK). For RNPs and ssODN-RNPs, the microscope sample carrier slides were coated using 0.01% poly-L-lysine. In a typical experiment, 10  $\mu$ L of clean D-PBS(–) was added to the well for focusing so that a silicone gasket (Refeyn, Ltd, Oxford,

UK) mounted on the washed microscope sample carrier slide could better find the glass/buffer interface. Ten  $\mu$ L of either Cas9 (5 nM), RNP (20 nM), or ssODN-RNP (20 nM) diluted with clean D-PBS(–) was mixed with the above 10  $\mu$ L of D-PBS (–) by pipetting, and movies were immediately recorded for 60 s at 48 frames per second (fps) under standard instrument settings. MP measurements were calibrated by contrast comparison with known mass calibrants including IgG (150 kDa) and bovine serum albumin (66 kDa) that were measured before each set of experiments. Sample molecular weights were obtained. All mass spectra are kernel-density estimates of the resultant histograms with the kernel having a Gaussian distribution.

### 3.6 Structural analysis using circular dichroism

Samples of sgRNAs, Cas9 proteins, and RNPs were measured using a JASCO J-820 circular dichroism spectropolarimeter (JASCO corporations, Tokyo, Japan). The sgRNAs were diluted with Milli-Q water to reach a volume of 9.9  $\mu$ M. Cas9 proteins and RNPs were diluted with Milli-Q water to a volume of 0.925  $\mu$ M. All spectra were recorded with the use of a 1 mm path length rectangular (10  $\times$  1) quartz cell (JASCO corporations) with the following settings: 190–330 nm spectral range, 50 nm  $\text{min}^{-1}$  scanning speed, 1 nm bandwidth, 0.5 nm data-capture intervals, 1 s response time, and 6 scans of accumulation. Finally, baseline and solvent corrections were performed using JASCO software.

### 3.7 Native polyacrylamide gel electrophoresis (PAGE)

Native-PAGE for sgRNAs was performed using a Mini-PROTEAN Tetra Vertical Electrophoresis Cell (Bio-Rad Laboratories, Inc., San Francisco, USA). Then, 100 ng of sgRNA was added with a 6 $\times$  Loading of Buffer Orange G (Nippon Gene Co., Ltd, Tokyo, Japan) and was then run in Mini-PROTEAN TGX Gels (4–15%) (Bio-Rad Laboratories) in Tris/Glycine buffer (2.5 mM Tris, 19.2 mM Glycine (pH 8.3) (Bio-Rad Laboratories)) at 100 V for 100 min. Gels were stained with SYBR Green II Nucleic Acid Gel Stain (TaKaRa Bio Inc., Shiga, Japan) and visualized with a Printgraph CMOS I (ATTO Corporation, Tokyo, Japan).

Native-PAGE for RNPs was performed using an M RapiDus Mini-Slab Electrophoresis Tank (ATTO Corporation). Four  $\mu$ g of RNPs was added with Loading Buffer (62.5 mM Tris, 40% Glycerol (pH 6.8)) and was then run in u-PAGE H (5%) (ATTO Corporation) in Tris/Glycine buffer (2.5 mM Tris, 19.2 mM Glycine (pH 8.3) (Bio-Rad Laboratories, Inc.)) at 120 V for 3–4 h. Gels were stained either with SYBR Green II Nucleic Acid Gel Stain (TaKaRa Bio Inc.) or EzStain Aqua (ATTO Corporation) for either sgRNA or Cas9 protein, respectively, and visualized using a Printgraph CMOS I (ATTO Corporation).

### 3.8 *In vitro* DNA cleavage assay

Purified genomic DNA (gDNA) was obtained, as described previously.<sup>39</sup> Five molar equivalents of RNP was added to the purified PCR product in reaction buffer (50 mM Tris-HCl, 100 mM NaCl, 10 mM MgCl<sub>2</sub>, 1 mM dithiothreitol, pH 7.9) and was

then incubated either for 1 h at 37 °C or for 8 h at 15 °C. Following heat inactivation of the Cas9 RNP at 65 °C for 5 min, 50 ng of the dsDNA was run in 3% agarose gel at 100 V for 40 min, stained with GelRed (Biotium, Inc., CA, USA) and visualized with a Printgraph CMOS I (ATTO Corporation). The bands were quantified using Image J software. DNA cleavage was calculated using the following formula.

$$\text{DNA cleavage} = \text{Int}_{\text{cleaved}} / \text{Int}_{\text{full+cleaved}}$$

In that formula, Int<sub>full</sub> and Int<sub>cleaved</sub> indicate intensity derived from full length (uncleaved) and cleaved DNA, respectively.

### 3.9 Animals

The experimental protocols were all reviewed and approved by the Hokkaido University Animal Care Committee under the guidelines for the care and use of laboratory animals (approval number: 20-0176). BALB/c mice (female, either 4 weeks old or pregnant) were purchased from Japan SLC (Shizuoka, Japan). Mice were maintained with an enrichment regimen (Shepherd Shack, Shepherd Specialty Papers, TN, USA) on a regular 12-hour light/12-hour dark cycle in a specific animal facility at Hokkaido University. Four to five mice were housed in each cage. The mice were fed a pelleted mouse diet (5053 – PicoLab® Rodent Diet 20, LabDiet, MO, USA) and water *ad libitum*.

### 3.10 Measurement of serum TTR protein levels

Mice were intravenously injected with Cas9/sgTTR RNP-loaded LNPs at the indicated dose. The mice were euthanized at the indicated timepoint after the injection, and blood was collected, clotted at room temperature for 1 h, and serum was isolated by centrifugation (25 °C, 1000g, 15 min). The TTR protein concentration in serum was determined using a Prealbumin ELISA Kit (mouse) (Aviva Systems Biology, CA, USA) according to the manufacturer's protocol.

### 3.11 Observation of intrahepatic distribution

Mice were intravenously injected with 0.2% DiD-labeled LNPs at a dose of 2.0 mg RNP kg<sup>-1</sup>. Ten minutes before the collection of liver tissues, blood vessels were stained by an intravenous injection of 20  $\mu$ g of fluorescein-labeled Tomato lectin (Vector Laboratories, Inc., CA, USA). Liver tissues were collected 60 min after the injection of the LNPs. The liver tissues were excited with 488 and 638 nm of light using an LU4 4-laser unit. The intrahepatic distribution of the LNPs was observed using a Nikon A1 (Nikon Co. Ltd, Tokyo, Japan) equipped with an objective lens (Plan Apo 40 $\times$  0.95NA DIC M/N2) and a dichroic mirror (DM 405/488/561/640). The three fluorescence detection channels (Ch) were set to the following filters: Ch1,525BP50 for fluorescein-labeled Tomato lectin and Ch2,700BP75 for DiD-labeled LNPs.

### 3.12 Statistical analysis

Results are expressed as the mean + the SD of independent experiments. For comparisons between the means of two variables, unpaired Student's *t* tests were performed. For compari-

sons between multiple groups, one-way analysis of variance (ANOVA) followed by Tukey or Dunnett's *post hoc* testing was performed. Group size, definition of center, and dispersion and precision measures are also noted in the figure legends as appropriate. All statistics were completed using GraphPad Prism software version 10.1.2 (San Diego, CA, USA).

## 4. Conclusions

In this study, we investigated the effects that the structural heterogeneity of sgRNA exert on the physical properties and activity of Cas9 RNP-loaded LNP formulations. The thermal denaturation of sgRNA resulted in the formation of uniform monomers, which led to a significant improvement in the yield of monomeric RNPs and to an increase in the density of the negative charge. Furthermore, these developments significantly improved the uniformity, RNP encapsulation efficiency, and the *in vivo* knockout activity of the RNP-loaded LNPs. Additionally, the resultant RNP-loaded LNPs proved to be resistant to cryopreservation and capable of inducing obvious gene knockouts in neonatal mice. These results suggest potential applications for RNP-loaded LNP formulations in the treatment of genetic diseases.

## Author contributions

Conceptualization and methodology: Y. S.; validation: Y. S.; formal analysis: R. S., M. S. and Y. S.; investigation: R. S. and Y. S.; resources: S. K., M. M., M. T., K. M. and Y. S.; writing – original draft: R. S. and Y. S.; writing – review & editing: Y. K., M. H., S. K., M. M., M. T., K. M., T. O., Y. Y. and H. H.; visualization: R. S. and Y. S.; supervision: Y. S.; project administration: Y. S.; funding acquisition: M. S., M. T., H. H. and Y. S. All authors have given approval to the final version of the manuscript.

## Conflicts of interest

There are no conflicts to declare.

## Data availability

The data supporting this article are included in the supplementary information (SI) and dataset.

Supplementary methods; Physicochemical properties of the LNPs; Sequences of sgRNAs; ssODNs; Capillary electrophoresis of sgTTR-G211; Native-PAGE of denatured sgTTR-G211 before and after freeze-thaw cycles; Native-PAGE of *in vitro* transcribed sgTTR-G211; Native-PAGE of several sgRNAs; Whole images of cryo-TEM observation; Bleb counts of cryo-TEM observation; Molecular weight distribution of RNPs targeting PCSK9; Molecular distribution of ssODN-RNPs; Molecular distribution of RNPs with different stoichiometries of sgRNA;

BN-PAGE of RNPs; Native-PAGE of RNPs; Molecular weight distribution of Cas9 protein; Native-PAGE of sgRNA denatured at different temperature; NanoFCM analyses of RNP-loaded LNPs. Supplementary information is available. See DOI: <https://doi.org/10.1039/d5pm00189g>.

## Acknowledgements

This work was supported, in part, by JSPS KAKENHI Grant Numbers JP23K19418, JP20H05873, JP24H00038, JP23K28421, and JP23H05451; by AMED Grant Numbers 24bm1223004s0502, and JP223fa627005; by the Hokkaido University Biosurface Project; and by the Takeda Science Foundation. The authors wish to thank Shin-Etsu Chemical Co., Ltd for kindly providing glass-based iLiNP microfluidic devices. The authors wish to thank Dr James L. McDonald for his helpful advice in preparing the English manuscript.

## References

- 1 M. Jinek, K. Chylinski, I. Fonfara, M. Hauer, J. A. Doudna and E. Charpentier, *Science*, 2012, **337**, 816–821.
- 2 Y. Zheng, Y. Li, K. Zhou, T. Li, N. J. VanDusen and Y. Hua, *Signal Transduction Targeted Ther.*, 2024, **9**, 47.
- 3 M. Pacesa, O. Pelea and M. Jinek, *Cell*, 2024, **187**, 1076–1100.
- 4 L. Cong, F. A. Ran, D. Cox, S. Lin, R. Barretto, N. Habib, P. D. Hsu, X. Wu, W. Jiang, L. A. Marraffini and F. Zhang, *Science*, 2013, **339**, 819–823.
- 5 H. X. Zhang, Y. Zhang and H. Yin, *Mol. Ther.*, 2019, **27**, 735–746.
- 6 C. A. Tsuchida, K. M. Wasko, J. R. Hamilton and J. A. Doudna, *Proc. Natl. Acad. Sci. U. S. A.*, 2024, **121**, e2307796121.
- 7 C. E. Nelson, C. H. Hakim, D. G. Ousterout, P. I. Thakore, E. A. Moreb, R. M. Castellanos Rivera, S. Madhavan, X. Pan, F. A. Ran, W. X. Yan, A. Asokan, F. Zhang, D. Duan and C. A. Gersbach, *Science*, 2016, **351**, 403–407.
- 8 N. E. Bengtsson, J. K. Hall, G. L. Odom, M. P. Phelps, C. R. Andrus, R. D. Hawkins, S. D. Hauschka, J. R. Chamberlain and J. S. Chamberlain, *Nat. Commun.*, 2017, **8**, 14454.
- 9 S. Shahin, H. Xu, B. Lu, A. Mercado, M. K. Jones, B. Bakondi and S. Wang, *Pharmaceutics*, 2022, **14**, 824.
- 10 M. Thürkauf, S. Lin, F. Oliveri, D. Grimm, R. J. Platt and M. A. Rüegg, *Nat. Commun.*, 2023, **14**, 6116.
- 11 Z. Wu, H. Yang and P. Colosi, *Mol. Ther.*, 2010, **18**, 80–86.
- 12 W. L. Chew, M. Tabebordbar, J. K. Cheng, P. Mali, E. Y. Wu, A. H. Ng, K. Zhu, A. J. Wagers and G. M. Church, *Nat. Methods*, 2016, **13**, 868–874.
- 13 V. Louis Jeune, J. A. Joergensen, R. J. Hajjar and T. Weber, *Hum. Gene Ther:Methods*, 2013, **24**, 59–67.
- 14 Y. Zhang, C. Sun, C. Wang, K. E. Jankovic and Y. Dong, *Chem. Rev.*, 2021, **121**, 12181–12277.



15 L. Duan, K. Ouyang, X. Xu, L. Xu, C. Wen, X. Zhou, Z. Qin, Z. Xu, W. Sun and Y. Liang, *Front. Genet.*, 2021, **12**, 673286.

16 J. D. Gillmore, E. Gane, J. Taubel, J. Kao, M. Fontana, M. L. Maitland, J. Seitzer, D. O'Connell, K. R. Walsh, K. Wood, J. Phillips, Y. Xu, A. Amaral, A. P. Boyd, J. E. Cehelsky, M. D. McKee, A. Schiermeier, O. Harari, A. Murphy, C. A. Kyratsous, B. Zambrowicz, R. Soltys, D. E. Gutstein, J. Leonard, L. Sepp-Lorenzino and D. Lebwohl, *N. Engl. J. Med.*, 2021, **385**, 493–502.

17 T. Wei, Q. Cheng, Y. L. Min, E. N. Olson and D. J. Siegwart, *Nat. Commun.*, 2020, **11**, 3232.

18 K. Chen, H. Han, S. Zhao, B. Xu, B. Yin, A. Lawanprasert, M. Trinidad, B. W. Burgstone, N. Murthy and J. A. Doudna, *Nat. Biotechnol.*, 2025, **43**, 1445–1457.

19 A. E. Briner, P. D. Donohoue, A. A. Gomaa, K. Selle, E. M. Slorach, C. H. Nye, R. E. Haurwitz, C. L. Beisel, A. P. May and R. Barrangou, *Mol. Cell*, 2014, **56**, 333–339.

20 R. Graf, X. Li, V. T. Chu and K. Rajewsky, *Cell Rep.*, 2019, **26**, 1098–1103.e3.

21 S. Riesenbergs, N. Helmbrecht, P. Kanis, T. Maricic and S. Pääbo, *Nat. Commun.*, 2022, **13**, 489.

22 J. Camperi, M. Moshref, L. Dai and H. Y. Lee, *Anal. Chem.*, 2022, **94**, 1432–1440.

23 I. C. Okafor and T. Ha, *J. Phys. Chem. B*, 2023, **127**, 45–51.

24 M. Halat, M. Klimek-Chodacka, J. Orleanska, M. Baranska and R. Baranski, *Int. J. Mol. Sci.*, 2021, **22**, 2937.

25 H. Nishimasu, F. A. Ran, P. D. Hsu, S. Konermann, S. I. Shehata, N. Dohmae, R. Ishitani, F. Zhang and O. Nureki, *Cell*, 2014, **156**, 935–949.

26 C. Anders, O. Niewoehner, A. Duerst and M. Jinek, *Nature*, 2014, **513**, 569–573.

27 F. Jiang, K. Zhou, L. Ma, S. Gressel and J. A. Doudna, *Science*, 2015, **348**, 1477–1481.

28 C. Huai, G. Li, R. Yao, Y. Zhang, M. Cao, L. Kong, C. Jia, H. Yuan, H. Chen, D. Lu and Q. Huang, *Nat. Commun.*, 2017, **8**, 1375.

29 S. B. Thyme, L. Akhmetova, T. G. Montague, E. Valen and A. F. Schier, *Nat. Commun.*, 2016, **7**, 11750.

30 J. D. Finn, A. R. Smith, M. C. Patel, L. Shaw, M. R. Youniss, J. van Heteren, T. Dirstine, C. Ciullo, R. Lescarbeau, J. Seitzer, R. R. Shah, A. Shah, D. Ling, J. Growe, M. Pink, E. Rohde, K. M. Wood, W. E. Salomon, W. F. Harrington, C. Dombrowski, W. R. Strapps, Y. Chang and D. V. Morrissey, *Cell Rep.*, 2018, **22**, 2227–2235.

31 A. Hendel, R. O. Bak, J. T. Clark, A. B. Kennedy, D. E. Ryan, S. Roy, I. Steinfeld, B. D. Lunstad, R. J. Kaiser, A. B. Wilkens, R. Bacchetta, A. Tselenko, D. Dellinger, L. Bruhn and M. H. Porteus, *Nat. Biotechnol.*, 2015, **33**, 985–989.

32 S. Kim, T. Koo, H. G. Jee, H. Y. Cho, G. Lee, D. G. Lim, H. S. Shin and J. S. Kim, *Genome Res.*, 2018, **28**, 367–373.

33 M. Kloczewiak, J. M. Banks, L. Jin and M. L. Brader, *Mol. Pharm.*, 2022, **19**, 2022–2031.

34 K. Suga, T. Tanabe, H. Tomita, T. Shimanouchi and H. Umakoshi, *Nucleic Acids Res.*, 2011, **39**, 8891–8900.

35 T. Miyahara, H. Nakatsuji and H. Sugiyama, *J. Phys. Chem. A*, 2016, **120**, 9008–9018.

36 M. Balcerowicz, M. Di Antonio and B. Y. W. Chung, *Bio-Protoc.*, 2021, **11**, e3950.

37 H. Onuma, R. Shimizu, Y. Suzuki, M. Sato, H. Harashima and Y. Sato, *iScience*, 2024, **27**, 110928.

38 Y. Suzuki, H. Onuma, R. Sato, Y. Sato, A. Hashiba, M. Maeki, M. Tokeshi, M. E. H. Kayesh, M. Kohara, K. Tsukiyama-Kohara and H. Harashima, *J. Controlled Release*, 2021, **330**, 61–71.

39 H. Onuma, Y. Sato and H. Harashima, *J. Controlled Release*, 2023, **355**, 406–416.

40 A. K. Leung, Y. Y. Tam, S. Chen, I. M. Hafez and P. R. Cullis, *J. Phys. Chem. B*, 2015, **119**, 8698–8706.

41 Y. Xu, A. Golubovic, S. Xu, A. Pan and B. Li, *J. Mater. Chem. B*, 2023, **11**, 6527–6539.

42 K. Mrksich, M. S. Padilla and M. J. Mitchell, *Adv. Drug Delivery Rev.*, 2024, **214**, 115446.

43 M. Jinek, K. Chylinski, I. Fonfara, M. Hauer, J. A. Doudna and E. Charpentier, *Science*, 2012, **337**, 816–821.

44 T. Karvelis, G. Gasiunas, A. Miksys, R. Barrangou, P. Horvath and V. Siksnys, *RNA Biol.*, 2013, **10**, 841–851.

45 M. Jinek, F. Jiang, D. W. Taylor, S. H. Sternberg, E. Kaya, E. Ma, C. Anders, M. Hauer, K. Zhou, S. Lin, M. Kaplan, A. T. Iavarone, E. Charpentier, E. Nogales and J. A. Doudna, *Science*, 2014, **343**, 1247997.

46 J. Snoeys, J. Lievens, E. Wisse, F. Jacobs, H. Duimel, D. Collen, P. Frederik and B. De Geest, *Gene Ther.*, 2007, **14**, 604–612.

47 Y. Sato, Y. Note, M. Maeki, N. Kaji, Y. Baba, M. Tokeshi and H. Harashima, *J. Controlled Release*, 2016, **229**, 48–57.

48 S. Li, C. Cortez-Jugo, Y. Ju and F. Caruso, *ACS Nano*, 2024, **18**, 33257–33263.

49 L. B. Harrington, D. Paez-Espino, B. T. Staahl, J. S. Chen, E. Ma, N. C. Kyriakis and J. A. Doudna, *Nat. Commun.*, 2017, **8**, 1424.

50 G. Paci, J. Caria and E. A. Lemke, *J. Cell Sci.*, 2021, **134**, jcs247874.

51 S. A. Adam, *Genome Biol.*, 2001, **2**, reviews0007.1.

52 I. Pudžiuvėlytė, K. Olechnovič, E. Godliauskaitė, K. Sermokas, T. Urbaitis, G. Gasiunas and D. Kazlauskas, *Bioinformatics*, 2024, **40**, btae157.

53 A. Singh, H. Irfan, E. Fatima, Z. Nazir, A. Verma and A. Akilimali, *Ann. Med. Surg.*, 2024, **86**, 4555–4559.

54 E. Oude Blenke, E. Örnskov, C. Schöneich, G. A. Nilsson, D. B. Volkin, E. Mastrobattista, Ö. Almarsson and D. J. A. Crommelin, *J. Pharm. Sci.*, 2023, **112**, 386–403.

55 K. Hashiba, M. Taguchi, S. Sakamoto, A. Otsu, Y. Maeda, H. Ebe, A. Okazaki, H. Harashima and Y. Sato, *Commun. Biol.*, 2024, **7**, 556.

56 M. Packer, D. Gyawali, R. Yerabolu, J. Schariter and P. White, *Nat. Commun.*, 2021, **12**, 6777.

57 C. Domingues, I. Jarak, F. Veiga, M. Dourado and A. Figueiras, *Pharmaceutics*, 2023, **15**, 2431.

58 S. Nishiwaki and Y. Ando, *Sci. Rep.*, 2020, **10**, 17145.



59 S. Hirota and T. Yamaguchi, *Clin. Pharmacol. Ther.*, 2020, **108**, 985–994.

60 A. A. Qureshi, B. Shaikh, A. S. Aswad, A. H. Saeed, H. Tabassum, M. F. Tahir and M. H. Jaber, *Ann. Med. Surg.*, 2024, **86**, 6376–6380.

61 P. Marks, *N. Engl. J. Med.*, 2025, **392**, 2271–2272.

62 K. Musunuru, S. A. Grandinette, X. Wang, T. R. Hudson, K. Briseno, A. M. Berry, J. L. Hacker, A. Hsu, R. A. Silverstein, L. T. Hille, A. N. Ogul, N. A. Robinson-Garvin, J. C. Small, S. McCague, S. M. Burke, C. M. Wright, S. Bick, V. Indurthi, S. Sharma, M. Jepperson, C. A. Vakulskas, M. Collingwood, K. Keogh, A. Jacobi, M. Sturgeon, C. Brommel, E. Schmaljohn, G. Kurgan, T. Osborne, H. Zhang, K. Kinney, G. Rettig, C. J. Barbosa, S. C. Semple, Y. K. Tam, C. Lutz, L. A. George, B. P. Kleinstiver, D. R. Liu, K. Ng, S. H. Kassim, P. Giannikopoulos, M. G. Alameh, F. D. Urnov and R. C. Ahrens-Nicklas, *N. Engl. J. Med.*, 2025, **392**, 2235–2243.

63 H. Wilton-Clark, E. Yan and T. Yokota, *Genes (Basel)*, 2024, **15**, 821.

64 L. Wang, Y. Yang, C. A. Breton, J. White, J. Zhang, Y. Che, A. Saveliev, D. McMenamin, Z. He, C. Latshaw, M. Li and J. M. Wilson, *Blood*, 2019, **133**, 2745–2752.

65 N. Kimura, M. Maeki, Y. Sato, Y. Note, A. Ishida, H. Tani, H. Harashima and M. Tokeshi, *ACS Omega*, 2018, **3**, 5044–5051.

66 K. Hashiba, M. Taguchi, S. Sakamoto, A. Otsu, Y. Maeda, Y. Suzuki, H. Ebe, A. Okazaki, H. Harashima and Y. Sato, *Nano Lett.*, 2024, **24**, 12758–12767.

